Remote sensing of aerosol properties from multi-wavelength and multi-pixel information over the ocean

Chong Shi[1,2,3] , Makiko Hashimoto[1], Teruyuki Nakajima[1]

[1]Japan Aerospace Exploration Agency, Earth Observation Research Center, Tsukuba, Ibaraki, 305-8505, Japan
5 [2]Key Laboratory of Meteorological Disaster of Ministry of Education, Nanjing University of Information Science and Technology, Nanjing, 210044, China
[3]Institute of Atmospheric Physics, Chinese Academy of Sciences, Beijing 100029, China.

Correspondence to: C. Shi (shi.chong@ac.jaxa.jp); T. Nakajima (nakajima.teruyuki@jaxa.jp)

Abstract. In this study, we investigate the feasibility of multi-pixel scheme in the inversion of aerosol optical thickness
10 (AOT) for multi-spectral satellite instruments over the ocean. Different from the traditional satellite aerosol retrievals
conducted pixel by pixel independently, we derive the aerosol optical thickness of multiple pixels simultaneously by adding
smoothness constraint on the spatial variation of aerosols and oceanic substances, which helps the satellite retrieval with
higher consistency from pixel to pixel. Simulations are performed for two representative oceanic circumstances—open and
coastal waters, as well as the land-ocean interface region. We retrieve the AOT for fine, sea spray, and dust particles
15 simultaneously using synthetic spectral measurements from the Greenhouse Gases Observing Satellite/Thermal and Near
Infrared Sensor for Carbon Observations-Cloud and Aerosol Imager (GOSAT/TANSO-CAI) with four wavelengths coving
from the ultraviolet to shortwave infrared bands. The forward radiation calculation is performed by a coupled
atmosphere-ocean radiative transfer model combined with a three-component bio-optical oceanic module, where the
chlorophyll *a* concentration, sediment and colored dissolved organic matter are considered. Results show that accuracies of
20 the derived AOT and spectral remote-sensing reflectance are both improved by applying smoothness constraints on the
spatial variation of aerosol and oceanic substances in homogeneous or inhomogeneous surface conditions. The multi-pixel
scheme can be effective to compensate the retrieval biases induced by measurement errors and improve the retrieval
sensitivity, particularly for the fine aerosol over the coastal water. We then apply the algorithm to derive AOTs using real
satellite measurements. Results indicate that the multi-pixel method helps to polish the irregular retrieved results of the
25 satellite imagery and shows promising potentiality to correct the overestimation of aerosols over high turbid waters, by
benefiting from the coincident retrieval of neighboring pixels. A comparison of retrieved AOTs from satellite measurements
with those from the Aerosol Robotic Network (AERONET) also indicates that retrievals conducted by the multi-pixel
scheme are more consistent with the AERONET observations.

Atmospheric
Chemistry
and Physics
Discussions

1 Introduction

Aerosols are one of the largest uncertainty factors in estimations and interpretations of the Earth's changing energy budget (Boucher et al., 2013). They exert significant and complex impacts on the radiation process through both direct and indirect

5   effects (Haywood and Boucher, 2000; Li et al., 2011), as well as having detrimental influences on the air quality and public health. Since the ocean covers more than 70 percent of the Earth's surface, it is indispensable to estimate the aerosol loading over the ocean. Due to the limitation of spatial and temporal coverage from ground-based measurements, satellite remote sensing has been the most efficient approach to observe the variation of aerosols over wide areas and with fine spatial-temporal resolution.

10   In the atmosphere-ocean system, the total radiance measured by a satellite-borne sensor at the top of atmosphere mostly comes from the atmospheric scattering, of which the oceanic contribution generally accounts for ~10% over open and non-glint ocean regions in or over the visible bands. In the 1990s, there are useful retrievals of aerosol optical thickness (AOT) over the global ocean derived from the Advanced Very High Resolution Radiometer (AVHRR) generated by NOAA (Stowe et al., 1992). Moreover, Nakajima and Higurashi (1997), and Mishchenko et al. (1999) propose an improved

15   two-channel method to derive more information of aerosols using red and near-infrared band (NIR) measurements from the AVHRR. With the advances in the satellite instrument, several improved algorithms have also been developed using more channels that cover band ranges from ultraviolet (UV) to NIR or shortwave infrared (SWIR) to retrieve both AOT and aerosol type (Tanré et al., 1997; Torres et al., 1998; Higurashi and Nakajima, 2002; Remer et al., 2005; Kim et al., 2007; Wang et al., 2017; Choi et al., 2018) or layer height (Xu et al., 2017). These algorithms have been successfully adopted in

20   the operational processing of aerosol retrieval for Polar or Geostationary satellite instruments with good accuracies. In addition, multiple angular or polarization measurements are conducive to derive aerosol properties by providing more information contents over the ocean (Mishchenko and Travis, 1997; Martonchik et al., 1998; Goloub et al., 1999). As for the ocean color (OC) retrieval, such as that used in the Sea Viewing Wide Field of View Sensor, atmospheric correction scheme is always adopted to derive AOT from sets of candidate aerosol modes based on the satellite measurements at red or NIR

25   channels (Gordon and Wang, 1994). Specifically, these approaches compare observed and pre-calculated radiances or polarized radiances from lookup tables to estimate aerosol optical properties assuming that the ocean surface reflectance can be empirically estimated or neglected. For example, the Moderate Resolution Imaging Spectroradiometer (MODIS) Collection 5 operational over-ocean algorithm specifies zero water-leaving radiance for all (550, 650, 860, 1240, 1600, and 2120 nm) except at 550 nm where a value of reflectance 0.005 is assumed (Remer et al., 2005). These assumptions are

30   generally reasonable due to the high absorption effect of seawater in or beyond the NIR bands so that the ocean surface can be assumed to be black. However, there is still about 50% discrepancy of the mean AOT from several prominent aerosol products over ocean, with the differences appearing both in terms of magnitude and temporal tendency (Li et al., 2009).

Apart from the different calibration or cloud screening schemes used in different algorithms, correction of the surface effect is one of the main factors causing such discrepancy (Li et al., 2009). As for the aerosol retrieval at shorter bands or in turbid waters, the backscattering of oceanic particulates could be higher, as a result that contributions from underwater field to the satellite observed reflectance should be accounted for. To further consider the effects of oceanic substances in the retrieval of

5   aerosols, other studies have been conducted to simultaneously derive AOT and water-leaving radiance using coupled atmosphere-ocean radiative transfer models (Doerffer and Fischer, 1994; Stamnes et al., 2003; Fan et al., 2017; Shi and Nakajima, 2018) or a sea surface reflectance model (Sayer et al., 2010), as well as the combined polarization information (Hasekamp et al., 2011; Knobelspiesse et al., 2012; Ottaviani et al., 2013; Gao et al., 2018).

Like most satellite retrievals, the aerosol inversions are performed over single pixel one at a time before moving to another

10   pixel, independently. To overcome the deficiency of the possibly limited information contained in a single pixel regarding all the retrieved parameters, Dubovik et al. (2011) develop a generalized aerosol retrieval system known as the Generalized Retrieval of Aerosol and Surface Properties (GRASP) to derive aerosol properties, which uses polarization, multi-angle, multi-wavelength, multi-pixel information integrated into a sophisticated statistically optimized scheme, based on the assumption that the variations of retrieved parameters are horizontally and temporally smooth from pixel to pixel and/or day

15   to day. A similar horizontal constraint scheme based on the adjacent pixel information has also been adopted in the retrieval of aerosol and water-leaving radiance over the open ocean (Xu et al., 2016). Since these algorithms adopt polarization and multi-angle measurements that many imagers cannot provide, Hashimoto and Nakajima (2017) develop a satellite remote-sensing algorithm to retrieve aerosol properties using multi-wavelength and multi-pixel information (MWMP). Adhering to the implementation of Hashimoto and Nakajima (2017) who implement aerosol retrieval over land, in this study,

20   we investigated the potential value of multi-pixel scheme combined with multiple wavelength information in the remote sensing of aerosols over several oceanic conditions, i.e., both open and coastal waters, as well as the land-ocean interface region.

In this study, we firstly use a well-established coupled atmosphere–ocean radiative transfer model to simulate the spectral measurements of the Greenhouse Gases Observing Satellite/Thermal and Near Infrared Sensor for Carbon

25   Observations-Cloud and Aerosol Imager (GOSAT/TANSO-CAI, hereafter referred as CAI) in four bands for two cases of open and coastal waters. Statistical samples of the MODIS ocean color data selected from two representative regions in the Lanai and Yellow Sea, are adopted to model the underwater optical properties in the simulation retrieval experiment. Then, we use the optimal estimation theory to investigate the effects of the multi-pixel scheme on the retrieval of aerosols by studying various numerical results in different ocean conditions. Finally, we conduct the retrievals based on the real CAI

30   measurements and make comparisons with those from the MODIS standard aerosol products and *in situ* observations from the Aerosol Robotic NETwork (AERONET) (Holben et al., 1998; Dubovik and King, 2000).

Atmospheric
Chemistry
and Physics
Discussions

2. Methodology

In the atmosphere and ocean system, the satellite-received multi-spectral radiance or reflectance vector at a subdomain of an imagery with multiple pixels can be expressed as $\mathbf{y}$, with the dimensions of $N_\lambda \times N_u \times N_v$, where N_λ is the number of measured wavelengths, and N_u and N_v are the numbers of pixels in two horizontal orthogonal directions of the

5   subdomain, respectively. The measurement vector can be related to the state vector $\mathbf{x}$ and error $\boldsymbol{\varepsilon}$ as follows:

$$\mathbf{y} = F(\mathbf{x}) + \boldsymbol{\varepsilon} \tag{1}$$

where $\mathbf{x}$ denotes the set of unknown parameters in the subdomain with the dimensions of $N_p \times N_u \times N_v$. Here, N_p is the number of parameters being retrieved in each single pixel and $F(\mathbf{x})$ is the forward radiative transfer model, which describes the knowledge of the measurement process and physics of the problem. $\boldsymbol{\varepsilon}$ is the error vector that consists of the

10   measurement and model errors. The inversion problem is to derive $\mathbf{x}$ from observations $\mathbf{y}$ by inverting the forward model F at a subdomain, i.e., simultaneous determination of the retrieved parameters with number of N_p in each pixel of the subdomain with dimensions of $N_u \times N_v$. Since the inversion is often an ill-posed problem, a prior constraint for the state vector is usually considered. Moreover, assuming the aerosol loading is a slowly variable function of the horizontal direction (Dubovik et al., 2011; Hashimoto and Nakajima, 2017), as is the chlorophyll *a* concentration (Chl) (Xu et al.,

15   2016), and extended to the sediment and colored dissolved organic matter (CDOM) which are more conspicuous in turbid waters, a spatial smoothness constraint on the variation of aerosol and oceanic substances can be added during the retrieval. If we treat the forward model as linear in the vicinity of the true state, the inversion tends to solve the equation set as follows:

$$\begin{cases} \mathbf{y} = \mathbf{K}\mathbf{x} + \boldsymbol{\varepsilon} \\ \mathbf{x} = \mathbf{x}_a + \boldsymbol{\varepsilon}_a \\ \mathbf{0} = \mathbf{B}_u + \mathbf{D}_u \mathbf{x} + \boldsymbol{\varepsilon}_u \\ \mathbf{0} = \mathbf{B}_v + \mathbf{D}_v \mathbf{x} + \boldsymbol{\varepsilon}_v \end{cases} \tag{2}$$

20   where $\mathbf{K}$ is the Jacobian matrix expressing the sensitivity of the model to an infinitesimal change in each retrieved parameter as $\mathbf{K} = \partial \mathbf{y} / \partial \mathbf{x}$, $\mathbf{x}_a$ is the apriori estimate of the state vector before retrieval, and $\boldsymbol{\varepsilon}_a$ is the apriori error. $\mathbf{B}_u$, $\mathbf{B}_v$ are the boundary conditions of which values are determined from the neighboring subdomains; $\mathbf{D}_u$, $\mathbf{D}_v$ comprise second differential coefficient matrix given by the Phillips–Twomey method (Phillips, 1962; Twomey, 1963), which are adopted as a smoothing constraint in each horizontal direction of the subdomain, and $\boldsymbol{\varepsilon}_u$ and $\boldsymbol{\varepsilon}_v$ indicate the uncertainties

25   of these derivatives in the u and v directions, respectively. It should be noted that this type of smoothing constraint has also been commonly used in the retrieval of aerosol size distribution derived from the ground-based measurements of AERONET and SKYNET (King et al., 1978; Nakajima et al., 1996; Dubovik and King, 2000). Provided that the

measurement and apriori error are characterized by a Gaussian probability distribution function, the inversion can be changed to minimize the cost function, as follows:

$$\phi = (\mathbf{y} - \mathbf{Kx})^{\mathrm{T}} \mathbf{S}_{\varepsilon}^{-1} (\mathbf{y} - \mathbf{Kx}) + (\mathbf{x} - \mathbf{x}_a)^{\mathrm{T}} \mathbf{S}_a^{-1} (\mathbf{x} - \mathbf{x}_a) +$$
$$\gamma_u (\mathbf{B}_u + \mathbf{D}_u \mathbf{x})^{\mathrm{T}} (\mathbf{B}_u + \mathbf{D}_u \mathbf{x}) + \gamma_v (\mathbf{B}_v + \mathbf{D}_v \mathbf{x})^{\mathrm{T}} (\mathbf{B}_v + \mathbf{D}_v \mathbf{x}) \tag{3}$$

where γ_u and γ_v denote Lagrange multipliers, which represent the strength of the spatial smoothness constraint on the norm of the second derivatives in two horizontal directions. In principle, these two parameters are interpreted by the reciprocal of the covariance of the horizontal distribution variation of the state vector, whereby the larger the Lagrange multiplier is, the stronger the smoothing constraint is. $\mathbf{S}_{\varepsilon}$ is the measurement error covariance matrix and $\mathbf{S}_a$ is the variance–covariance matrix estimated by apriori state values, of which the off-diagonal elements are assumed as 0. The optimal solution of Eq. (3) can be solved by the Gauss–Newton iteration method, as follows:

$$\mathbf{x}_{i+1} = \mathbf{x}_i + [(\mathbf{K}_i^{\mathrm{T}} \mathbf{S}_{\varepsilon}^{-1} \mathbf{K}_i + \mathbf{S}_a^{-1}) + (\gamma_u \mathbf{D}_u^{\mathrm{T}} \mathbf{D}_u + \gamma_v \mathbf{D}_v^{\mathrm{T}} \mathbf{D}_v)]^{-1} \cdot$$
$$[\mathbf{K}_i^{\mathrm{T}} \mathbf{S}_{\varepsilon}^{-1} (\mathbf{y} - \mathbf{K}_i \mathbf{x}_i) - \mathbf{S}_a^{-1} (\mathbf{x}_i - \mathbf{x}_a) - \gamma_u (\mathbf{D}_u^{\mathrm{T}} \mathbf{D}_u \mathbf{x}_i + \mathbf{D}_u^{\mathrm{T}} \mathbf{B}_u) - \gamma_v (\mathbf{D}_v^{\mathrm{T}} \mathbf{D}_v \mathbf{x}_i + \mathbf{D}_v^{\mathrm{T}} \mathbf{B}_v)] \tag{4}$$

with

$$\mathbf{D} = \begin{bmatrix} -2\mathbf{I} & \mathbf{I} & & & \\ \mathbf{I} & -2\mathbf{I} & \mathbf{I} & & \mathbf{0} \\ & \ddots & \ddots & \ddots & \\ \mathbf{0} & & \mathbf{I} & -2\mathbf{I} & \mathbf{I} \\ & & & \mathbf{I} & -2\mathbf{I} \end{bmatrix} \tag{5}$$

where $\mathbf{x}_i$ is the state vector to be retrieved at the i-th iteration of the subdomain and $\mathbf{I}$ is the unit matrix with a size of N_p. After several iterations, the retrieved parameters over multiple pixels at the subdomain can be converged and derived simultaneously. It should be noted that when the Lagrange multipliers, i.e., γ_u and γ_v, are 0, which means no spatial smoothness constraints are implemented in the retrieval, Eq. (4) is changed to the typical solution of the maximum a posteriori method used in the traditional single-pixel retrieval (Rodger, 2000).

3. Modeling of atmosphere-ocean system

In this study, we use a coupled atmosphere-ocean vector radiative transfer model, i.e., Pstar, for the forward radiation calculation (Ota et al., 2010). Pstar was originally developed for the simulation of radiative transfer in the coupled atmosphere-ocean system by accounting for the polarization effects. It is developed based on the scalar version of Rstar (Nakajima and Tanaka, 1986, 1988) and improved by Shi et al. (2016) to simulate the radiation process in turbid waters by combining a three-component bio-optical ocean module and water-leaving radiance calculation scheme. The accuracy of radiative transfer scheme in the model has been proved by a serious inter-comparison from IPRT (International Radiation

Atmospheric
Chemistry
and Physics
Discussions

Polarized Radiative Transfer) (Emda et al., 2015) in the atmosphere and the standard underwater radiative transfer problem in the ocean system provided by Mobley et al. (1993) (Shi et al., 2015).

For the aerosol mode, we adopted a sophisticated multicomponent scattering approach that combines external and internal mixture schemes, as well as the hygroscopic growth of each component. The external-mixture aerosol is assumed to consist of fine, sea spray, and dust particles combined with an internal mixture of water-soluble, dust-like and soot exists within the fine aerosols, of which the refractive index is calculated by the sum of each internal component contribution based on its volume fraction. It should be noted that the dust particles are considered as non-spherical, of which the scattering phase matrix is calculated using the Dubovik et al.'s (2002) method. Since CAI has only four spectral bands without multi-angle or polarization information, the size parameters for each particle are fixed in this study (Shettle and Robert, 1979) even though they differ from pixel to pixel in reality. However, a comprehensive retrieval experiment covering different ocean regions has demonstrated the reasonability of this assumption in the retrieval of AOT and water-leaving radiance based on the systematic comparison with those from AERONET-OC measurements (Shi and Nakajima, 2018).

For the ocean, we assume a four-layer system of infinite depth coupled with a wind-generated rough surface model, of which the reflectance and transmission matrices are calculated based on the scheme of Nakajima and Tanaka (1983). Moreover, a three-component bio-optical ocean module is implemented to model the inherent optical properties (IOPs) of oceanic substances, i.e., Chl, sediment and CDOM (Shi et al., 2016). To model the IOPs of seawater, particularly in the UV bands, we used newly compiled data from Lee et al. (2015), which have provided better closure for the remote sensing reflectance (Rrs), i.e., ratio between the water-leaving radiance and the downward irradiance just above the ocean surface, in the UV–visible domains. It should be noted that we use the Rrs instead of the water-leaving contribution to the satellite received radiance due to its important effect on the ocean color retrieval in this study.

4. Results and discussions

4.1. Retrieval using synthetic measurements

We focus on the retrieval from the GOSAT/TANSO-CAI. GOSAT is mainly designed to measure the carbon dioxide loading using the TANSO-Fourier Transform Spectrometer. In addition, the satellite carries the Cloud and Aerosol Imager (CAI) with four channels (380, 674, 870, and 1600 nm) covering from UV to SWIR bands for cloud screening and aerosol detection. We firstly simulate the synthetic measurements from CAI in four spectral bands ($N_\lambda = 4$) based on the improved Pstar model. Moreover, we define a 5×5 pixel region as one subdomain, i.e., $N_{u/v} = 5$, though there is no limitation in these definition if the computer resource is allowed. The geometries information are determined by the mean values of the CAI observations at solar zenith angle of 27°±1, satellite zenith angle of 30°±1 and relative azimuth angle of 150°±1 at the subdomain (Hashimoto and Nakajima, 2017).

The simulated true AOT values at 500 nm for each particle are given as 0.02, 0.1, 0.2 and 0.3, respectively. The total AOT is the sum of each AOT in a random mixture. We defined the soot fraction in fine particles as randomly ranging from 0.5% to 1.5%. In the ocean surface, a moderate wind speed of 5 m s^{-1} is assumed. From the widely used suite compiled by the NASA Ocean Biology Processing Group, and based on the large statistical ocean color sample of MODIS, we selected two

5   representative classes of oceanic scenarios: the Linai region, in which the water is typically clear with climatological values of Chl, a_443, and bbp_443 of about 0.056 mg m^{-3}, 0.017 m^{-1}, and 0.0014 m^{-1}, respectively; and the Yellow Sea, in which the water is typically coastal with climatological values of Chl, a_443, and bbp_443 of about 3.00 mg m^{-3}, 0.35 m^{-1} and 0.039 m^{-1}, respectively, where a_443 denotes the total absorption coefficient of ocean at 443nm and bbp_443 is the total backscattering coefficient of oceanic particulates at 443 nm. It should be noted that the used Chl products are derived by the

10   OCI algorithm of Hu et al. (2012) and a_443, bbp_443 products are derived by the QAA method of Lee et al. (2002), respectively. We assume the aerosol and oceanic-substance spatial distributions to be homogeneous in the 5×5 pixel regions. In total, we have 64 atmospheric cases of simulated observation data with Gaussian-random-noise of 2% standard deviation as measurement errors for each oceanic condition, then eight parameters of each pixel, i.e., AOTs of fine, sea spray, and dust particles; volume soot fraction in fine particles; wind speed; and concentrations of Chl, sediment, and CDOM

15   for the whole subdomain, are determined simultaneously using Eq. (4). The soot fraction in fine particles is defined as the retrieval parameter owing to its high absorption effects. The apriori conditions are randomly defined in a ±50% range of the true values, except for the soot fraction, which had a fixed value of 0.01. To investigate the feasibility of multi-pixel method in the retrieval, we analyzed the simulation data adopting different γ values of 0.0, 0.1, 0.5, 1.0, 1.5, 2.0, and 3.0. The general simulation and retrieval setup are summarized in Tables 1–2.

20   Figure 1 shows the retrieved AOT and spectral Rrs values with true conditions, as well as the statistical results of the retrieved relative error and root mean square deviation (RMSD) at different values of γ for the open ocean. Note that Figs. 1a–1g show only the retrievals of 0.0 and 3.0 at γ, which denote the use of no spatial smoothness constraint, i.e., the traditional single pixel method, and allowed a variation of about 1.35 times the retrieved parameters constrained from neighboring pixels, respectively. The results indicate that the accuracy of the retrieved AOT of each particle is generally

25   improved by using the spatial smoothness constraint, i.e., the multi-pixel method, to correct the retrieval bias induced by measurement errors. Specifically, the retrieved relative error and RMSD of the fine AOT decrease from 30.51% and 0.03109 to 13.45% and 0.01812, respectively, when the γ values change from 0.0 to 3.0 (Fig.1h and 1i), which indicates the effectiveness of the multi-pixel method in aerosol retrieval. Coarse aerosols (sum of sea spray and dust) can also be well derived, which is partly due to the adoption of the SWIR channel observation (Fig. 1e), even though larger errors are shown

30   for the inversion of each coarse aerosol, i.e., AOT of sea spray and dust (Figs. 1b and 1c). Additionally, due to the more significant improvement in the retrieval of fine particles, the multi-pixel scheme contributes to a better estimation of the total AOT (Fig. 1f). In contrast, the soot fraction is difficult to retrieve due to its low sensitivity to measurements, even though an UV channel observation, i.e., 380 nm, is implemented by the CAI, for which the retrieval results are highly dependent on the

apriori value (1% in this case) (Fig. 1d). In regards to the spectral Rrs, we find the multi-pixel method helps to facilitate the consistency of the retrieval to the true values (Fig. 1g) in comparison to those derived by the single pixel method, and this finding is similar to that of Xu et al. (2016) over open oceans. The low values of Rrs at 860 nm and at 674 nm also support the reasonability of our previous black ocean assumption in those bands in the two-channel aerosol inversion (Nakajima and

5 Higurashi, 1997). However, the underwater influence in the retrieval of aerosols at UV channels over the open ocean is suggested to be considered due to the higher backscattering effect of ocean body.

Over coastal waters, the sediment and CDOM, which are existed with higher concentrations in the ocean and show generally similar inherent optical properties to the fine particles and soot, exert non-negligible effects on the aerosol retrieval. Compared with the inversion of fine AOT over the open ocean (Fig. 1a), the retrieval in the low-aerosol loading over coastal

10 regions shows larger biases when using the traditional single-pixel method, mainly due to the contamination of oceanic sediment (Fig. 2a). Nevertheless, retrieval errors can be effectively reduced using the multi-pixel scheme, with the relative error and RMSD decreasing about 27.4% and 0.02234 (Figs. 2k–2l), respectively, which denote more significant benefit of the multi-pixel strategy than those performed over the open ocean. This improvement is also due in part to the better estimation of the spectral Rrs (Fig. 2j). It is demonstrated that the retrieved accuracy of AOT for coarse particles is generally

15 similar to that in clear waters (Fig. 2e), which is partly attributable to the utilization of SWIR measurements that are not sensitive to sediment and can be used in the atmospheric correction over turbid waters (Wang and Shi, 2007). Moreover, it remains difficult to retrieve the absorptive soot over coastal waters even when using the multi-pixel constraint (Fig. 2d). With regard to the underwater retrieval, significant improvements are evident in the inversion of oceanic substances, particularly for the sediment and CDOM, after implementing the spatial smoothness constraint (Figs. 2g–2i). Such

20 improvements also contribute to the better retrieval of the spectral Rrs, with the relative errors in the first three CAI bands decreasing from 41.87%, 17.76%, and 15.94% to 22.87%, 8.09%, and 8.23%, respectively. Generally, there are higher averaged kernel matrix values for fine and coarse aerosols, sediment, and CDOM, than those for the soot fraction and Chl, as well as the wind speed in the non-glint cases during the retrieval. It should be noted that we used relatively accurate apriori values for the AOT estimation in a range of ±50% of the true conditions, however, the retrieved sea spray and dust will have

25 larger biases when $\mathbf{x}_a$ exceeds true values more largely, owing to the limited spectral information of CAI and similar optical properties of these two kinds particles. However, their sum, i.e., total coarse AOT, can be still well determined and exhibit no obvious dependence on the apriori conditions.

The above results demonstrate the effectiveness of the multi-pixel scheme in the retrieval of aerosols over homogeneous atmosphere–ocean areas. To consider the retrieval under inhomogeneous conditions, we conducted further inversion

30 experiments in two situations. First, we assumed the aerosol loading and oceanic substances change continuously from coastal to open ocean with a large spatial variation in the 5×5 pixel subdomain. Results indicate that the multi-pixel strategy still performs better retrieval in this case, as shown in Figs. 3a–3c, particularly for the estimation of fine aerosols. Similar to the retrievals over homogeneous region, the spectral Rrs can be better derived using the multi-pixel scheme,

especially over coastal regions (low values of Rrs at 380 nm and high values of Rrs at 674 nm), but the traditional single-pixel method tends to yield larger bias estimations for the retrieval (Fig. 3c). Another inversion experiment is performed for the retrieval over land (with a higher aerosol loading and soot fraction) and coastal ocean interface regions in the subdomain. In this simulation, the land surface is assumed as reddish-brown fine sandy loam with spectral reflectance

5   values of 0.1098, 0.2775, 0.3630, and 0.4790 for the four CAI bands, of which values are selected from ECOSTRESS spectral library (https://speclib.jpl.nasa.gov/library). For the aerosols retrieval over land, we make simultaneous determinations of the AOT and spectral surface reflectance (A_g) with randomly defined apriori values of A_g in a range of ±10% of the true conditions and assumed spectral uncertainties of 0.02, 0.02, 0.02, and 0.001 for the CAI channels, respectively. The results indicate that the single-pixel method generally overestimates the fine and coarse AOT values over

10   sand due to the high ground reflectance. However, the retrieval accuracy over sand surface improves significantly by constraining the spatial aerosol variation in the subdomain, which also benefits from the better AOT estimation over the coastal ocean region (Fig. 3d–3e). With regard to the retrieval of the soot fraction (SF) (Fig. 3f), it remains difficult to derive over ocean areas with a high dependence on the aprior value (red line of Fig. 3f), whereas absorptive soot can be better estimated over land regions due to the high reflectance of the ground surface by providing more significant information to

15   the retrieval. Moreover, the multi-pixel scheme promotes the inversion of the SF, particularly in high aerosol conditions, which is similar to the research of Hashimoto and Nakajima (2017) conducted over the whole land regions. The performance of retrieval for absorptive soot with dependence on the aerosol loading over the land, of which the better retrievals are identified in the condition of AOT of fine particles at 500 nm over 0.1 (Fig. 3f) in this study, also supports the finding that errors of retrieved single scattering albedo decrease with increasing AOT for the AERONET (Dubovik et al., 2000b). It is

20   interesting that the retrieved accuracy of SF nearest the coastal line over the ocean (solid circles of Fig. 3f) tends to be improved using the multi-pixel method, though it is slightly. This improvement is more significant in the homogeneous aerosol distribution and dominated fine particle conditions over the land-ocean interface region, just as Fig.4 shows. The availability in retrieving the absorptive soot over the dark surface, i.e., ocean region, benefits from the spatial smoothness constraint from the better derived SF over the bright surface, i.e., sand ground, where the surface albedo is near or over the

25   neutral reflectance defined by Kaufman (1987). We then derived the relationship between the neutral reflectance (A_n), as which the apparent reflectance does not change with AOT, and the single scattering albedo (ω), asymmetry factor (g), phase function ($P(\cos\Theta)$) of aerosols based on the single scattering and two-stream approximation over land, as follow,

$$A_n = \frac{\pi\omega P(\cos\Theta)}{\mu\mu_0[\hat{t}(\mu)+\hat{t}(\mu_0)]}; \quad \hat{t}(\mu) \equiv m[1-\omega\frac{1}{2}(1+\frac{3}{2}g\mu)] \tag{6}$$

where μ and μ_0 are the cosine of the satellite and solar zenith angle. It is demonstrated that the neutral reflectance of

30   band2 of the CAI is ranged from 0.232 to 0.275 when the asymmetry factor and phase function are 0.7 and 0.0142, respectively, corresponding to the single scattering albedo of 0.935 and 0.950 with the soot fraction of 2.05% and 5.10%,

which are generally similar to the threshold values of retrieved SF in Fig. 3(f) and 4(b). However, these threshold values are just the specific case used in this study and also dependent on the ratio of fine AOT in real conditions.

4.2. Retrieval using real CAI measurements

Following the simulation retrieval experiment performed using synthetic spectral measurements, we then apply the proposed
5   algorithm to the real CAI data for deriving aerosols over ocean. Radiometric correction was conducted as prescribed in Shiomi et al. (2010). With regards to the ancillary data, we use the surface pressure and wind speed data from the National Centers for Environmental Prediction (NCEP) to correct the Rayleigh scattering and sea surface reflectance, respectively, as well as the relative humidity data to account for the effect of aerosol hygroscopic growth. The gas absorption is processed by a correlated k-distribution approach (Sekiguchi and Nakajima, 2008) where several main absorptive gases are considered, of
10   which the column ozone data is adopted from the Ozone Monitoring Instrument (OMI). In particular, we used a relatively high spatial smoothness constraint with γ value of 1.0 for each horizontal orthogonal direction in the multi-pixel scheme. Moreover, to keep the consistency between each subdomain, the boundary conditions of $\mathbf{B}_{u/v}$ used in Eq. (4) are determined by the retrieved results derived from the neighbor subdomains.

Figure 5 compares the spatial distributions of retrieved AOT for fine, coarse (sum of sea spray and dust), and total particles
15   using single- and multi-pixel methods. Results show that the derived AOTs by the single-pixel approach have a generally similar spatial distribution to those retrieved by the multi-pixel method, of which the fine aerosol dominates. However, irregular dotted variations with abnormal retrieval results are shown in some pixels (black box of Fig. 5) when conducting the single-pixel retrieval. Although it is difficult to support these irregular dotted distributions to be real, the investigation of the posterior error in those pixels demonstrates that the retrieved uncertainties are generally higher than those of other pixels
20   (not shown). Such kind of occasionally irregular dotted variation derived by the single-pixel method has also been identified in the aerosol retrieval over land (Hashimoto and Nakajima, 2017), which we rather consider it is caused by errors in the single-pixel inversion that tends to be affected by various observation noises. On the contrary, the multi-pixel scheme is more robust to these factors that the irregular dotted variation of retrieved AOT can be effectively improved when considering the spatial smoothness constraint during the retrieval, just as Fig. 5d–5f shown, which allows reduction of the
25   retrieval errors constrained by adjacent pixels.

Another retrieval experiment is performed on the monitoring of the Asian dust event from the CAI. Studies have demonstrated that dust aerosols carried by the dust storm in East Asia exert significant influence on the local ecosystem and environmental pollution (Mikami et al., 2006; Huang et al., 2014). Figure 6 shows the spatial distribution of retrieved AOT of fine and coarse particles from CAI on the April 27th, 2012, over the Yellow Sea. In order to have a better validation for
30   current algorithm, the MODIS standard Level 2 aerosol products derived using more channels, with the satellite overpass time about 3 hours later than that of the CAI, are also adopted as comparison. Results show that a relatively obvious transport belt for fine aerosols between the south of Shandong Peninsula and the middle of Yellow Sea is derived by the CAI

(Fig. 6a), meanwhile, significant dust storms are determined in the north of Yellow Sea (Fig. 6d), of which the retrieved coarse AOTs at 500 nm are over 1.5 in the high density areas. It is indicated that the derived AOTs for fine and coarse particles are generally consistent to the MODIS standard aerosol products with similar spatial distributions (Fig. 6c and 6f). In addition, the derived AOTs from CAI by the multi-pixel method (Fig. 6b and 6e) around the Shandong Peninsula are in

5   more agreement with MODIS aerosol products than those retrieved by the single-pixel approach, which implies the effectiveness of the multi-pixel scheme in the inversion of aerosols, particularly for fine particles. It should be noted that the derived fine AOT values from CAI seems to be generally lower than those obtained using MODIS products over the Yellow Sea. Although our algorithm divides the coarse particles into sea spray and yellow sand, it is more convinced to use their sum, i.e., coarse AOT, than the yellow sand as the indicator of the Asian dust transport, since the retrieval errors of coarse

10   AOT determined by the CAI are much lower than those of individual yellow sand, just as Fig. 2c and 2e showed. Such deficiency in distinguishing the sea spray and dust is expected to be better improved using the upcoming Cloud and Aerosol Image 2 (CAI2) with seven channels (340, 380, 443, 550, 674, 869 and 1630 nm) by providing more measurement information.

Retrieval of aerosols over extremely high turbid waters is still challenging problem due to the significant contamination from

15   the backscattering of oceanic particulates currently. Taking the Hangzhou Bay (HZB) as a sample region, the total suspended particulate matter can be over 1000 mg l^{-1} sometimes (He et al., 2013), which contributes a substantial proportion into the satellite signals, as a result that the aerosol is generally difficult to be accurately derived. In order to investigate the feasibility of multi-pixel scheme in the retrieval of AOT over high turbid water, we try to apply current algorithm in such circumstance. Figure 7 shows the comparison of retrieved total AOT by single- and multi-pixel method with or without

20   using SWIR band of CAI, i.e., 1600nm, with those from the MODIS aerosol products on December March, 2013, over the East China Sea. It should be noted that there are several high-error observation belts for band 4 in this image (Fig. 7f) due to some instrument problems, but the data are available to most regions including HZB. Results demonstrated that the retrieved AOTs by the CAI with or without using the SWIR measurement are all consistent to those of the MODIS aerosol product (Fig. 7c) beyond the coastlines, however, the estimated AOTs from CAI using different strategies around high turbid regions

25   show large differences. Generally, the derived AOTs without using SWIR measurements (Fig. 7a) demonstrate obvious overestimations than those retrieved adding SWIR information (Fig. 7d), especially near HZB region. Although we also simultaneously conduct the oceanic sediment retrieval in the algorithm, it is still difficult to use 3 spectral measurements to estimate at least 5 free variables (AOT of fine, sea spray and dust, sediment and CDOM) in the high backscattering surface condition, where the retrieval could be degenerated. Nevertheless, the deficiency of overestimation for the derived AOTs can

30   be effectively improved when adding SWIR observation during the retrieval (Fig. 7d), since satellite reflectance at SWIR band is much less sensitive to the suspended sediment than those of aerosols. Moreover, such deficiency can be also improved using the multi-pixel scheme even though the SWIR measurements are not used (Fig. 7b), which indicates the potentiality of multi-pixel strategy in the aerosol retrieval over high turbid waters, particularly for those multi-spectral instruments without the SWIR observation.

To further investigate the feasibility of this algorithm, two *in situ* data from the AERONET, i.e., Ieodo_Station and Gageocho_Station, are used for the validation. To examine the dependence of this retrieval on the apriori information, we set fixed values of $\mathbf{x}_a$ for all cases. We selected the retrieved state vector from the pixel closest to the AERONET site in the subdomain. The results indicate that the retrieved AOT values for fine and coarse aerosols, as well as the total aerosols, are

5 all consistent with those of the AERONET observations without significant dependence on the apriori information (Fig. 8). It should be noted that the simultaneous retrieved AOTs for fine and coarse aerosols are denoted in same color. Generally, increased accuracy in the determination of AOTs is demonstrated by using the multi-pixel method (shown by circles), with the retrieved relative errors of AOT for fine, coarse and total aerosols decrease from 26.19%, 96.70%, and 27.64% to 23.52%, 86.83% and 22.40%, as well as the RMSD varied from 0.1062, 0.05660 and 0.1129 to 0.06838, 0.04960 and

10 0.08738, respectively, in comparison to those derived by the single-pixel scheme (shown by crosses). As in the simulation inversion experimental results shown in Figures 1–3, the multi-pixel scheme tends to be more effective in the retrieval of fine than of coarse aerosols from the CAI measurements. However, we still identify few cases in which the retrieved errors have increased using the multi-pixel scheme, which inspires us to make further studies on the better definition of γ values for each retrieved parameter or the pixel resolution of subdomain.

15 **5. Conclusions and outlooks**

In this work, we focused on the aerosol retrieval from multi-pixel and multi-spectral satellite observations from CAI over the ocean. Unlike most algorithms that conduct the aerosol retrieval pixel by pixel, we derive aerosol properties of multiple pixels simultaneously by considering the smoothness constraint on the spatial variation of aerosols and oceanic substances between the pixels, i.e., multi-pixel method. We firstly investigated the availability of the multi-pixel scheme in the

20 conditions of open and coarse ocean, as well as the land-ocean interface region based on the synthetic measurements of CAI. Results indicate that the multi-pixel scheme improves the aerosol inversion by increasing the retrieval sensitivity and correcting the retrieval bias induced by measurement errors over multiple pixels, particularly for the fine aerosol over coastal regions. In addition, the spectral remote-sensing reflectance can be also derived in a higher accuracy by constraining the spatial variation of components in the ocean. We then apply current algorithm using real CAI measurements. The image

25 analysis demonstrates that the irregular retrieved results can be effectively improved using the spatial smoothness constraint. In addition, the multi-pixel scheme shows promising potentiality to retrieve the aerosols over high turbid waters, especially for those instruments without SWIR measurements. In comparisons with the AERONET observation, retrievals using multi-pixel scheme tend to be more consistent to the measurements than those derived by the single-pixel method.

Although we compared retrievals using different Lagrange multipliers values in this study, it is noted that these parameters

30 have similar roles of covariance of retrieved state vector and should be decided by observed variables or information from high-resolution instruments for the spatial smoothness constraint, which needs more analysis. Since CAI is mainly designed

Atmospheric
Chemistry
and Physics
Discussions

to determine the cloud and aerosol information, it is appropriate to examine the multi-pixel approach in the retrieval of ocean color using real satellite data. Moreover, investigation regarding the multi-pixel scheme's retrieval performance over the sunglint area, is also a part of our future work. Actually, the retrieved results shown in Fig. 6 are contaminated by the sunglint to some extent, with the glint angles mostly ranging from 25° to 40° of the imagery. As our previous study that

5   simultaneous adjustment of the wind speed value helps the aerosol retrieval over the sunglint region by correcting the surface reflectance (Shi and Nakajima, 2018), the retrieved AOT of fine and coarse aerosols from CAI show general consistency to those of MODIS products without sunglint contamination (Fig. 6). Nevertheless, it seems that the retrieved AOTs of fine particles are still lower than those of the MODIS products overall, which also inspires us to make a further study on the application of multi-pixel scheme in this issue.

10   **Acknowledgements**

References

Boucher, O., et al. (2013), Clouds and aerosols, in Climate change 2013: The physical science basis. Contribution of working group I to the fifth assessment report of the intergovernmental panel on climate change, edited, pp. 571-657, Cambridge University Press, Cambridge, United Kingdom and New York, NY, USA, 571–657, 2013.

25   Choi, M., J. Kim, J. Lee, M. Kim, B. Holben, T. F. Eck, Z. Li, and C. H. Song (2018), GOCI Yonsei aerosol retrieval version 2 products: an improved algorithm and error analysis with uncertainty estimation from 5-year validation over East Asia, Atmos. Meas. Tech., 11(1), 385.

Doerffer, R., and J. Fischer (1994), Concentrations of chlorophyll, suspended matter, and gelbstoff in case II waters derived from satellite coastal zone color scanner data with inverse modeling methods, J. Geophys. Res.: Oceans (1978–2012),

30   99(C4), 7457-7466.

Atmospheric
Chemistry
and Physics
Discussions

Dubovik, O., and M. D. King (2000a), A flexible inversion algorithm for retrieval of aerosol optical properties from Sun and sky radiance measurements, J. Geophys. Res.-Atmos. (1984–2012), 105(D16), 20673-20696.

Dubovik, O., A. Smirnov, B. Holben, M. King, Y. Kaufman, T. Eck, and I. Slutsker (2000b), Accuracy assessments of aerosol optical properties retrieved from Aerosol Robotic Network (AERONET) Sun and sky radiance measurements, J.

5   Geophys. Res.-Atmos., 105(D8), 9791-9806.

Dubovik, O., B. Holben, T. Lapyonok, A. Sinyuk, M. Mishchenko, P. Yang, and I. Slutsker (2002), Non-spherical aerosol retrieval method employing light scattering by spheroids, Geophys. Res. Lett., 29(10).

Dubovik, O., M. Herman, A. Holdak, T. Lapyonok, D. Tanré, J. Deuzé, F. Ducos, A. Sinyuk, and A. Lopatin (2011), Statistically optimized inversion algorithm for enhanced retrieval of aerosol properties from spectral multi-angle polarimetric

10 satellite observations, Atmos. Meas. Tech., 4(20), 975-1018.

Emde, C., V. Barlakas, C. Cornet, F. Evans, S. Korkin, Y. Ota, L. C. Labonnote, A. Lyapustin, A. Macke, and B. Mayer (2015), IPRT polarized radiative transfer model intercomparison project–Phase A, J. Quant. Spectrosc. Ra., 164, 8-36.

Fan, Y., W. Li, C. K. Gatebe, C. Jamet, G. Zibordi, T. Schroeder, and K. Stamnes (2017), Atmospheric correction over coastal waters using multilayer neural networks, Remote Sens. Environ., 199, 218-240.

15 Gao, M., P.-W. Zhai, B. Franz, Y. Hu, K. Knobelspiesse, P. J. Werdell, A. Ibrahim, F. Xu, and B. Cairns (2018), Retrieval of aerosol properties and water-leaving reflectance from multi-angular polarimetric measurements over coastal waters, Opt. Express, 26(7), 8968-8989.

Goloub, P., D. Tanre, J.-L. Deuze, M. Herman, A. Marchand, and F.-M. Bréon (1999), Validation of the first algorithm applied for deriving the aerosol properties over the ocean using the POLDER/ADEOS measurements, IEEE Trans. Geosci.

20 Remote Sens., 37(3), 1586-1596.

Gordon, H. R., and M. Wang (1994), Retrieval of water-leaving radiance and aerosol optical thickness over the oceans with SeaWiFS: a preliminary algorithm, Appl. Optics, 33(3), 443-452.

Hasekamp, O. P., P. Litvinov, and A. Butz (2011), Aerosol properties over the ocean from PARASOL multiangle photopolarimetric measurements, J. Geophys. Res.-Atmos., 116, doi:10.1029/2010jd015469.

25 Hashimoto, M., and T. Nakajima (2017), Development of a remote sensing algorithm to retrieve atmospheric aerosol properties using multi-wavelength and multi-pixel information, J. Geophys. Res.-Atmos., 6347-6378.

Haywood, J., and O. Boucher (2000), Estimates of the direct and indirect radiative forcing due to tropospheric aerosols: A review, Rev. Geophys., 38(4), 513-543.

He, X. Q., Y. Bai, D. L. Pan, N. L. Huang, X. Dong, J. S. Chen, C. T. A. Chen, and Q. F. Cui (2013), Using geostationary

30 satellite ocean color data to map the diurnal dynamics of suspended particulate matter in coastal waters, Remote Sens. Environ., 133, 225-239, doi:10.1016/j.rse.2013.01.023.

Higurashi, A., and T. Nakajima (2002), Detection of aerosol types over the East China Sea near Japan from four-channel satellite data, Geophys. Res. Lett., 29(17).

Atmospheric
Chemistry
and Physics
Discussions

Holben, B., T. Eck, I. Slutsker, D. Tanre, J. Buis, A. Setzer, E. Vermote, J. Reagan, Y. Kaufman, and T. Nakajima (1998), AERONET—A federated instrument network and data archive for aerosol characterization, Remote Sens. Environ., 66(1), 1-16.

Hu, C., Z. Lee, and B. Franz (2012), Chlorophyll a algorithms for oligotrophic oceans: A novel approach based on
5   three-band reflectance difference, J. Geophys. Res.: Oceans, 117(C1).

Huang, J., T. Wang, W. Wang, Z. Li, and H. Yan (2014), Climate effects of dust aerosols over East Asian arid and semiarid regions, J. Geophys. Res.-Atmos., 119(19), 11,398-311,416.

Kaufman, Y. J. (1987), Satellite sensing of aerosol absorption, J. Geophys. Res.-Atmos., 92(D4), 4307-4317.

Knobelspiesse, K., B. Cairns, M. Mishchenko, J. Chowdhary, K. Tsigaridis, B. van Diedenhoven, W. Martin, M. Ottaviani,
10   and M. Alexandrov (2012), Analysis of fine-mode aerosol retrieval capabilities by different passive remote sensing instrument designs, Opt. Express, 20(19), 21457-21484.

Kim, J., J. Lee, H. C. Lee, A. Higurashi, T. Takemura, and C. H. Song (2007), Consistency of the aerosol type classification from satellite remote sensing during the Atmospheric Brown Cloud–East Asia Regional Experiment campaign, J. Geophys. Res.-Atmos., 112(D22).

15   King, M. D., D. M. Byrne, B. M. Herman, and J. A. Reagan (1978), Aerosol size distributions obtained by inversions of spectral optical depth measurements, J. Atmos. Sci., 35(11), 2153-2167.

Lee, Z., J. Wei, K. Voss, M. Lewis, A. Bricaud, and Y. Huot (2015), Hyperspectral absorption coefficient of "pure" seawater in the range of 350–550 nm inverted from remote sensing reflectance, Appl. Optics, 54(3), 546-558.

Lee, Z., K. L. Carder, and R. A. Arnone (2002), Deriving inherent optical properties from water color: a multiband
20   quasi-analytical algorithm for optically deep waters, Appl. Optics, 41(27), 5755-5772.

Li, Z., F. Niu, J. Fan, Y. Liu, D. Rosenfeld, and Y. Ding (2011), Long-term impacts of aerosols on the vertical development of clouds and precipitation, Nat. Geosci., 4(12), 888-894.

Li, Z., X. Zhao, R. Kahn, M. Mishchenko, L. Remer, K. Lee, M. Wang, I. Laszlo, T. Nakajima, and H. Maring (2009), Uncertainties in satellite remote sensing of aerosols and impact on monitoring its long-term trend: a review and perspective,
25   Ann. Geophys, 27(7), 2755-2770.

Martonchik, J. V., D. J. Diner, R. A. Kahn, T. P. Ackerman, M. M. Verstraete, B. Pinty, and H. R. Gordon (1998), Techniques for the retrieval of aerosol properties over land and ocean using multiangle imaging, IEEE Trans. Geosci. Remote Sens., 36(4), 1212-1227.

Mikami, M., G. Shi, I. Uno, S. Yabuki, Y. Iwasaka, M. Yasui, T. Aoki, T. Tanaka, Y. Kurosaki, et al. (2006), Aeolian dust
30   experiment on climate impact: An overview of Japan–China joint project ADEC, Glob Planet Change, 52(1-4), 142-172.

Mishchenko, M. I., and L. D. Travis (1997), Satellite retrieval of aerosol properties over the ocean using polarization as well as intensity of reflected sunlight, J. Geophys. Res., 102(D14), 16989-17013.

Mishchenko, M. I., I. V. Geogdzhayev, B. Cairns, W. B. Rossow, and A. A. Lacis (1999), Aerosol retrievals over the ocean by use of channels 1 and 2 AVHRR data: sensitivity analysis and preliminary results, Appl. Optics, 38(36), 7325-7341.

Atmospheric
Chemistry
and Physics
Discussions

Mobley, C. D., B. Gentili, H. R. Gordon, Z. Jin, G. W. Kattawar, A. Morel, P. Reinersman, K. Stamnes, and R. H. Stavn (1993), Comparison of numerical models for computing underwater light fields, Appl. Optics, 32(36), 7484-7504.

Nakajima, T., and A. Higurashi (1997), AVHRR remote sensing of aerosol optical properties in the Persian Gulf region, summer 1991, J. Geophys. Res.-Atmos. (1984–2012), 102(D14), 16935-16946.

Nakajima, T., G. Tonna, R. Rao, P. Boi, Y. Kaufman, and B. Holben (1996), Use of sky brightness measurements from ground for remote sensing of particulate polydispersions, Appl. Optics, 35(15), 2672-2686.

Nakajima, T., and M. Tanaka (1983), Effect of wind-generated waves on the transfer of solar radiation in the atmosphere-ocean system, J. Quant. Spectrosc. Ra., 29(6), 521-537.

Nakajima, T., and M. Tanaka (1986), Matrix formulations for the transfer of solar radiation in a plane-parallel scattering atmosphere, J. Quant. Spectrosc. Ra., 35(1), 13-21.

Nakajima, T., and M. Tanaka (1988), Algorithms for radiative intensity calculations in moderately thick atmospheres using a truncation approximation, J. Quant. Spectrosc. Ra., 40(1), 51-69.

Ota, Y., A. Higurashi, T. Nakajima, and T. Yokota (2010), Matrix formulations of radiative transfer including the polarization effect in a coupled atmosphere–ocean system, J. Quant. Spectrosc. Ra., 111(6), 878-894.

Ottaviani, M., K. Knobelspiesse, B. Cairns, and M. Mishchenko (2013), Information content of aerosol retrievals in the sunglint region, Geophys. Res. Lett., 40(3), 631-634.

Phillips, D. L. (1962), A technique for the numerical solution of certain integral equations of the first kind, JACM, 9(1), 84-97.

Remer, L. A., Y. Kaufman, D. Tanré, S. Mattoo, D. Chu, J. V. Martins, R.-R. Li, C. Ichoku, R. Levy, and R. Kleidman (2005), The MODIS aerosol algorithm, products, and validation, J. Atmos. Sci., 62(4), 947-973.

Rodgers, C. D. (2000), Inverse methods for atmospheric sounding: Theory and practice, World scientific, Singapore.

Sayer, A., G. Thomas, and R. Grainger (2010), A sea surface reflectance model for (A) ATSR, and application to aerosol retrievals, Atmos. Meas. Tech., 3, 813-838.

Sekiguchi, M., and T. Nakajima (2008), A k-distribution-based radiation code and its computational optimization for an atmospheric general circulation model, J. Quant. Spectrosc. Ra., 109(17), 2779-2793.

Shettle, E. P., and R. W. Fenn (1979), Models for the aerosols of the lower atmosphere and the effects of humidity variations on their optical properties, Air Force Geophysics Laboratory, Hanscom Air Force Base, Mass., 1979.

Shi, C., P. Wang, T. Nakajima, Y. Ota, S. Tan, and G. Shi (2015), Effects of Ocean Particles on the Upwelling Radiance and Polarized Radiance in the Atmosphere–Ocean System, Adv. Atmos. Sci., 32, 1-11.

Shi, C., and T. Nakajima (2018), Simultaneous determination of aerosol optical thickness and water leaving radiance from multispectral measurements in coastal waters, Atmos. Chem. Phys., 18(6), 3865-3884.

Shi, C., T. Nakajima, and M. Hashimoto (2016), Simultaneous retrieval of aerosol optical thickness and chlorophyll concentration from multiwavelength measurement over East China Sea, J. Geophys. Res.-Atmos., 121, 14084-14101.

Shiomi, K., S. Kawakami, and T. Kina (2010), Operation results of initial calibration and validation of "IUBKI" [in Japanese], Aeronaut. Space Sci. Jpn., 58, 158–163.

Stamnes, K., W. Li, B. Yan, H. Eide, A. Barnard, W. S. Pegau, and J. J. Stamnes (2003), Accurate and self-consistent ocean color algorithm: simultaneous retrieval of aerosol optical properties and chlorophyll concentrations, Appl. Optics, 42(6),
5   939-951.

Stowe, L., R. Carey, and P. Pellegrino (1992), Monitoring the Mt. Pinatubo aerosol layer with NOAA/11 AVHRR data, Geophys. Res. Lett., 19(2), 159-162.

Tanré, D., Y. Kaufman, M. Herman, and S. Mattoo (1997), Remote sensing of aerosol properties over oceans using the MODIS/EOS spectral radiances, J. Geophys. Res.-Atmos., 102(D14), 16971-16988.

10   Torres, O., P. Bhartia, J. Herman, Z. Ahmad, and J. Gleason (1998), Derivation of aerosol properties from satellite measurements of backscattered ultraviolet radiation: Theoretical basis, J. Geophys. Res.-Atmos. (1984–2012), 103(D14), 17099-17110.

Twomey, S. (1963), On Numerical Solution Of Fredholm Integral Equations Of First Kind By Inversion Of Linear System Produced By Quadrature, JACM, 10(1), doi:10.1145/321150.321157.

15   Wang, M., and W. Shi (2007), The NIR-SWIR combined atmospheric correction approach for MODIS ocean color data processing, Opt. Express, 15(24), 15722-15733.

Wang, Y., J. Wang, R. C. Levy, X. Xu, and J. S. Reid (2017), MODIS Retrieval of Aerosol Optical Depth over Turbid Coastal Water, Remote Sens., 9(6), 595.

Xu, F., Dubovik, O., Zhai, P.-W., Diner, D. J., Kalashnikova, O. V., Seidel, F. C., Litvinov, P., Bovchaliuk, A., Garay, M. J.,
20   van Harten, G., and Davis, A. B.: Joint retrieval of aerosol and water-leaving radiance from multispectral, multiangular and polarimetric measurements over ocean, Atmos. Meas. Tech., 9, 2877– 2907.

Xu, X., J. Wang, Y. Wang, J. Zeng, O. Torres, Y. Yang, A. Marshak, J. Reid, and S. Miller (2017), Passive remote sensing of altitude and optical depth of dust plumes using the oxygen A and B bands: First results from EPIC/DSCOVR at Lagrange-1 point, Geophys. Res. Lett., 44(14), 7544-7554.

Atmospheric
Chemistry
and Physics
Discussions

Table 1. Aerosol and Oceanic mode Used in This Study

		External mixture	Internal mixture	Spherical	Height (km)	Median radius (μm)[a]	Standard deviation[a]	True values
Atmosphere		Fine	Water-soluable, dust-like, soot	Yes	0 ~ 2	0.175	0.806	0.02, 0.1, 0.2, 0.3
		Sea spray	Sea salt	Yes	0 ~ 2	2.200	0.698	0.02, 0.1, 0.2, 0.3
		Dust	Yellow sand	No	4 ~ 8	4.000	1.099	0.02, 0.1, 0.2, 0.3
			Chl (mg m^{-3})	Sediment (g m^{-3})	CDOM (m^{-1})	a_443 (m^{-1})	bbp_443 (m^{-1})	
Ocean		Clear waters (Linai)	0.056	0.060	0.0035	0.017	0.0014	
		Coastal waters (Yellow Sea)	3.000	1.800	0.2500	0.350	0.0390	

[a]The volume size distribution of aerosol particles is assumed to follow a lognormal function as

$$\frac{dV}{d\ln r} = \frac{V}{\sqrt{2\pi}}\exp[-\frac{(\ln r - \ln r_{mv})^2}{2\sigma_v^2}]$$, where V is the aerosol volume density, r_{mv} is the median radius, and σ_v is the

standard deviation.

5

Atmospheric
Chemistry
and Physics
Discussions

Table 2. Retrieval experiment sets for state vector and measurement for the CAI

	Retrieved parameter	Initial value	Apriori value[b]	Apriori uncertainty[b]	Horizontal constraint	Lagrange multiplier
Atmosphere	AOT_fine[a]	0.01	±50%x_t	0.3	Yes	0.0, 0.1, 0.5, 1.0, 1.5, 2.0, 3.0
	AOT_seaspray[a]	0.01	±50%x_t	0.3	Yes	0.0, 0.1, 0.5, 1.0, 1.5, 2.0, 3.0
	AOT_dust[a]	0.01	±50%x_t	0.3	Yes	0.0, 0.1, 0.5, 1.0, 1.5, 2.0, 3.0
	Soot fraction	0.01	0.01	0.02	Yes	0.0, 0.1, 0.5, 1.0, 1.5, 2.0, 3.0
Ocean	Wind speed	3.0	±50%x_t	3.0	Yes	0.0, 0.1, 0.5, 1.0, 1.5, 2.0, 3.0
	Chl	0.03	±50%x_t	5.0x_t	Yes	0.0, 0.1, 0.5, 1.0, 1.5, 2.0, 3.0
	Sediment	0.001	±50%x_t	6.0x_t	Yes	0.0, 0.1, 0.5, 1.0, 1.5, 2.0, 3.0
	CDOM	0.01	±50%x_t	5.0x_t	Yes	0.0, 0.1, 0.5, 1.0, 1.5, 2.0, 3.0
	Band1	Band2		Band3	Band4	
Observation error	2% Gaussian Random error	2% Gaussian Random error		2% Gaussian Random error	2% Gaussian Random error	
Error covariance matrix	$[\ln(1+2\%)]^2$	$[\ln(1+2\%)]^2$		$[\ln(1+2\%)]^2$	$[\ln(1+2\%)]^2$	

[a]AOT refers to the aerosol optical thickness at 500nm; [b]x_t is the true value defined in this simulation
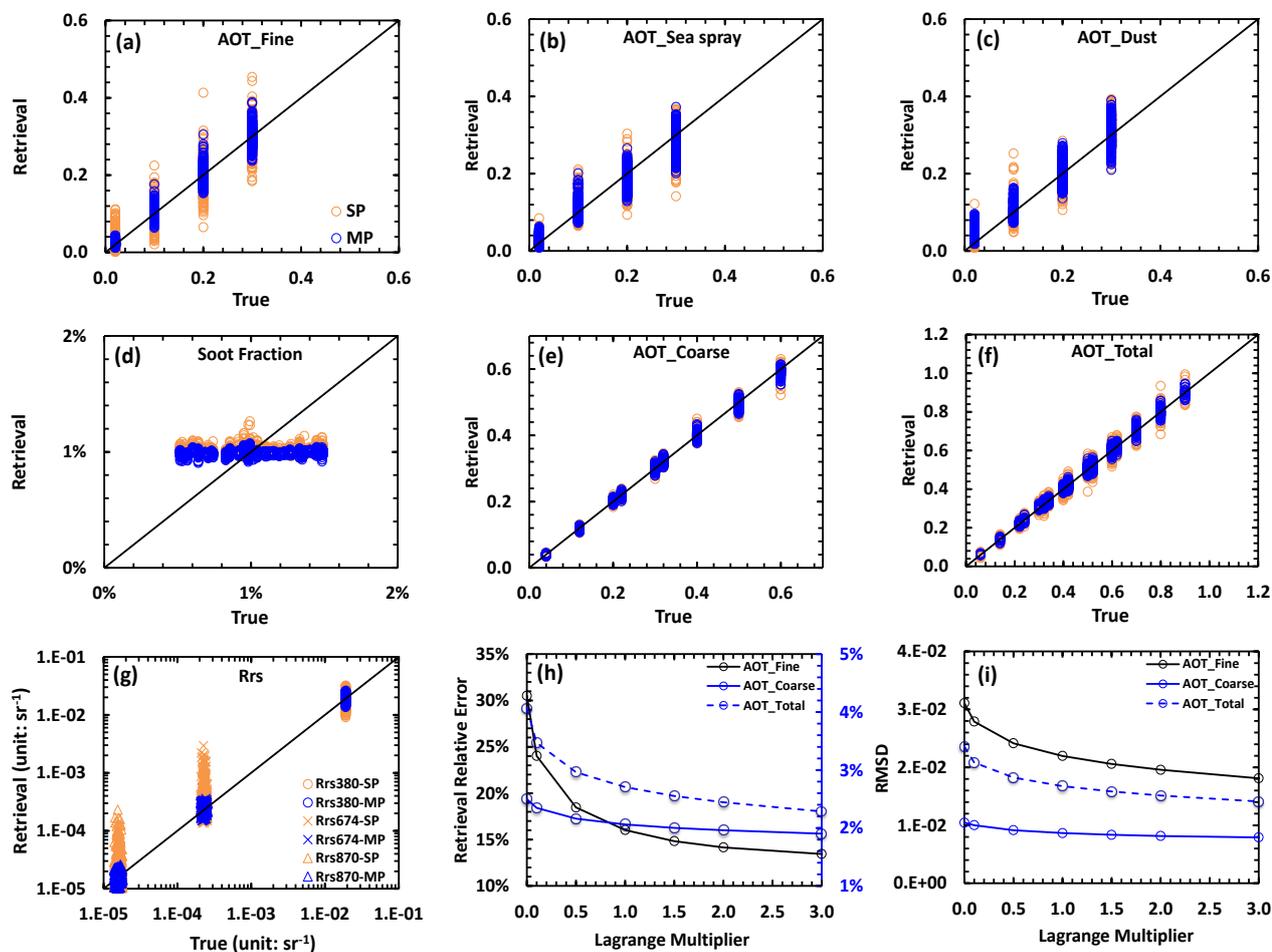
Figure 1: Retrieved and true AOT values over homogeneous open-ocean areas for fine (a), sea spray (b), dust (c), coarse i.e., sum of sea spray and dust (e), and total i.e., sum of fine, sea spray, and dust (f) particles, at 500 nm, as well as the soot fraction (d) and spectral remote-sensing reflectance (Rrs) (g) for Lagrange multipliers of 0.0 (i.e., single-pixel method, as characterized by "SP") and 3.0 (i.e., multi-pixel method, as characterized by "MP"). Retrieved relative error (h) and root mean square error (RMSD) (i) are shown for each Lagrange multipliers values.
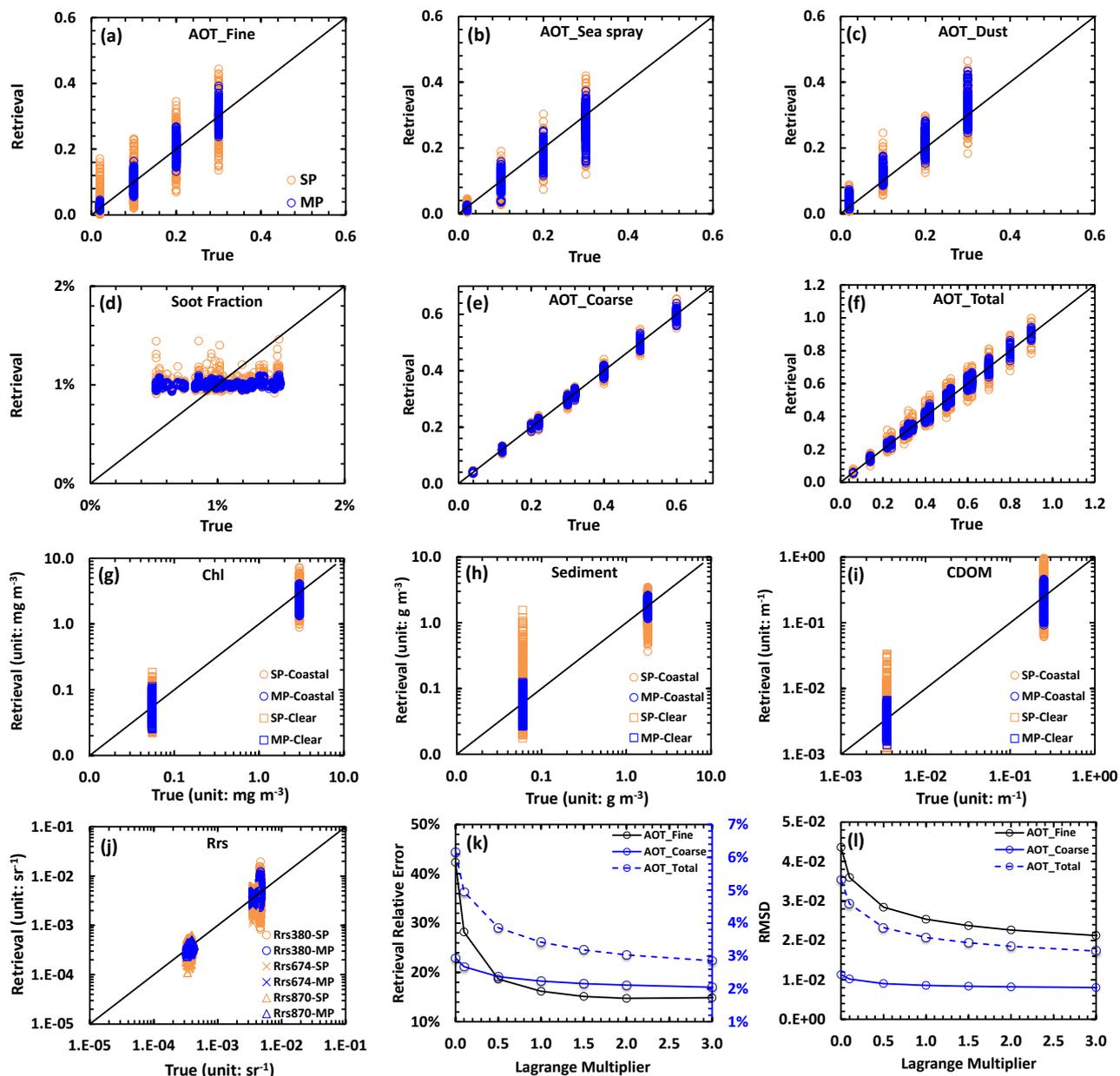
Figure 2: Same as in Figure 1 but for coastal waters

Atmospheric
Chemistry
and Physics
Discussions
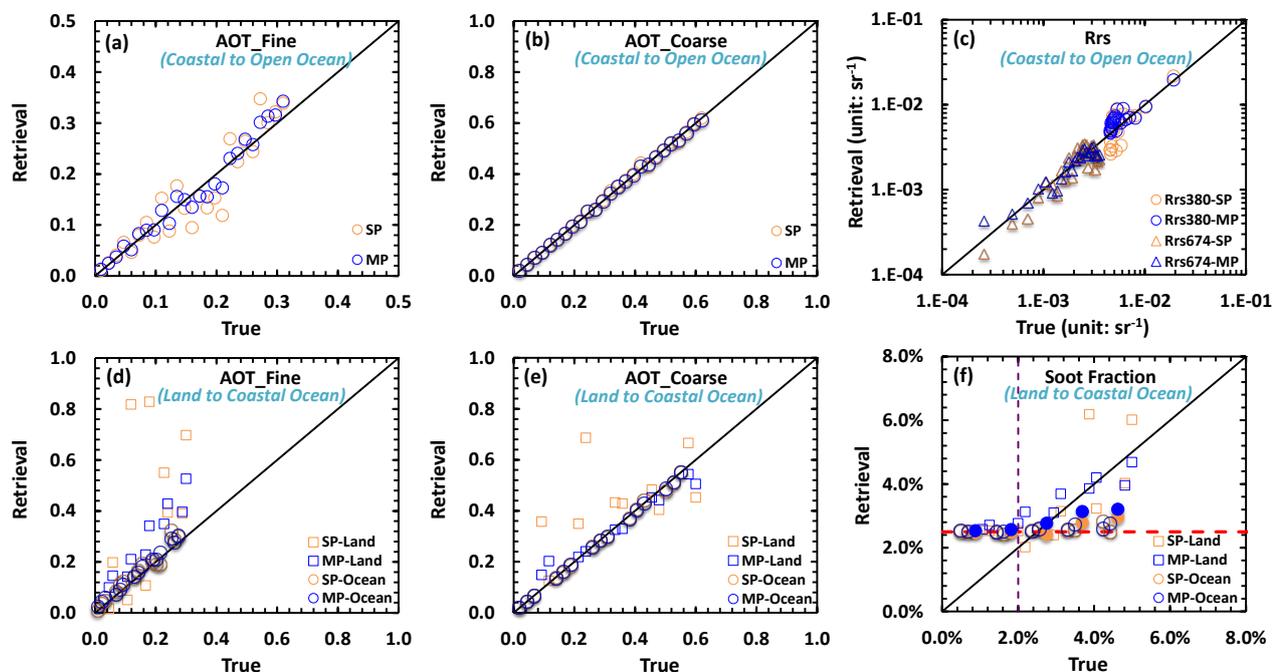
Figure 3: **Simulation experiment for AOT retrieval of fine and coarse aerosols, spectral Rrs with (blue points characterized by "MP" with γ values of 1.0) and without (orange points characterized by "SP") multi-pixel constraints over inhomogeneous areas from coastal to open ocean regions (a–c), and retrievals from land (ground covered by reddish-brown fine sandy loam) to coastal ocean regions (d–f). The purple line of (f) is the boundary line with AOT_Fine at 500 nm of 0.1 (right part of boundary line denotes retrieval under the condition of AOT_Fine greater than 0.1, and vice versa). The red line of (f) shows the apriori values used in this simulation. The retrieved soot fractions over ocean nearest the coastal line are denoted by solid circle in (f). Land surface reflectances at 380, 674, 870, and 1600 nm are 0.1098, 0.2775, 0.3630, and 0.4790, respectively.**

Atmospheric
Chemistry
and Physics
Discussions
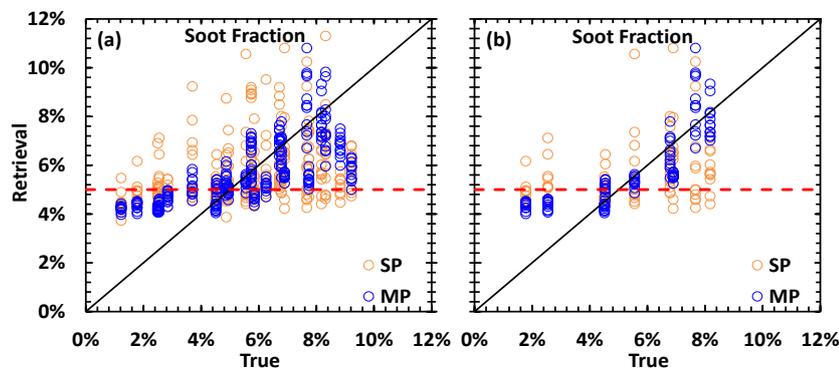
Figure 4: **Retrieved volume soot fraction in the fine aerosol over the coastal ocean with the condition of homogeneous aerosol distribution for the land-ocean interface region. (a) is the retrieval with AOT of fine > 0.1; (b) is the retrieval with AOT of fine > 0.1 and ratio of fine AOT > 0.5. The red line shows the apriori values used in this simulation.**
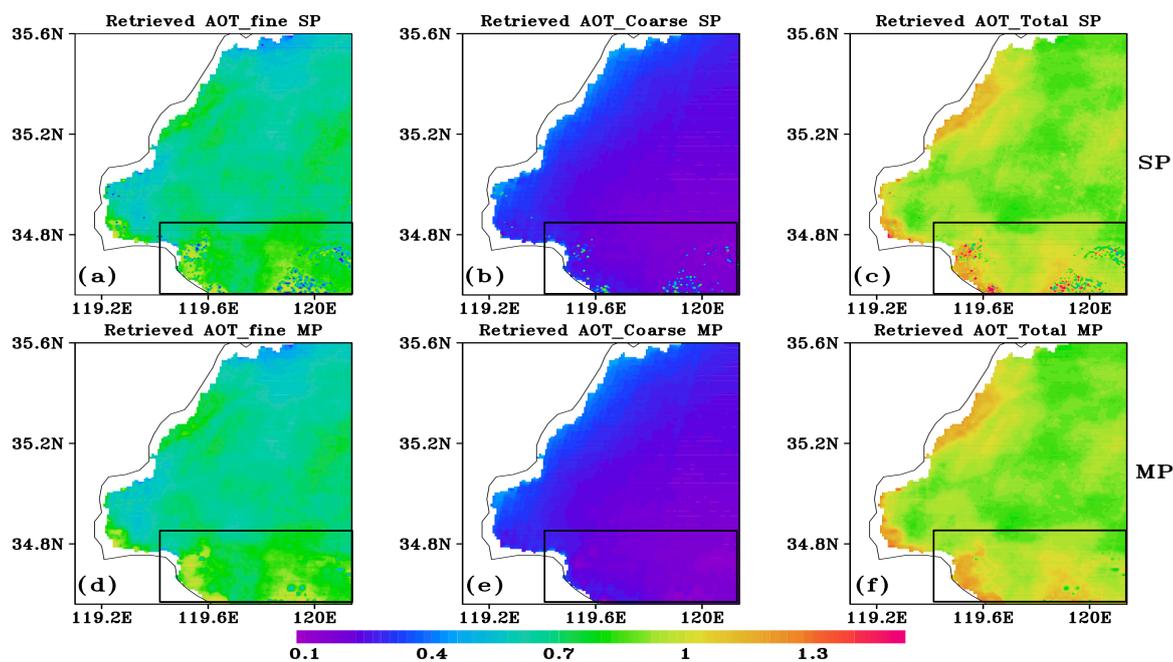
Figure 5: **Spatial distributions of retrieved AOT for fine, coarse, and total particles from CAI measurement on 13th March 2012, using traditional single pixel method (characterized by "SP") and multi-pixel scheme (characterized by "MP").**
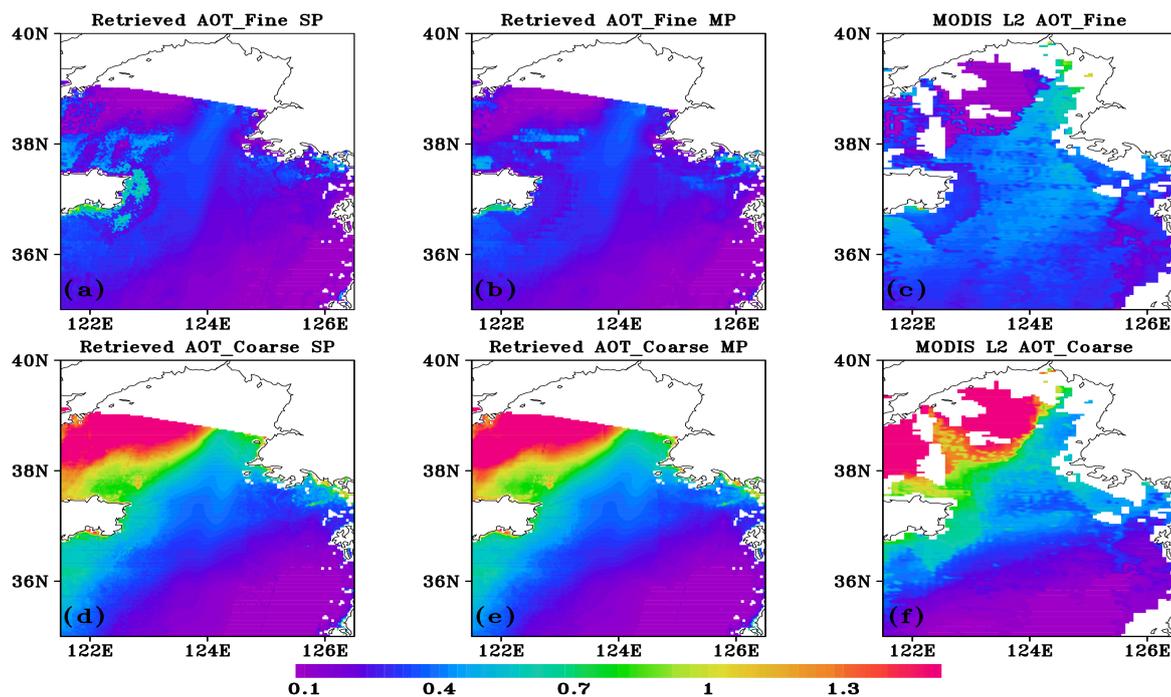
Figure 6: Monitoring of the Asian Dust event from CAI and MODIS. Spatial distribution of CAI-derived AOT for fine and coarse aerosols from the single-pixel method (a–b) and multi-pixel method (d–e), as well as the MODIS/Terra aerosol level 2 products (c and f) on the April 27th, 2012, over the Yellow Sea, respectively.
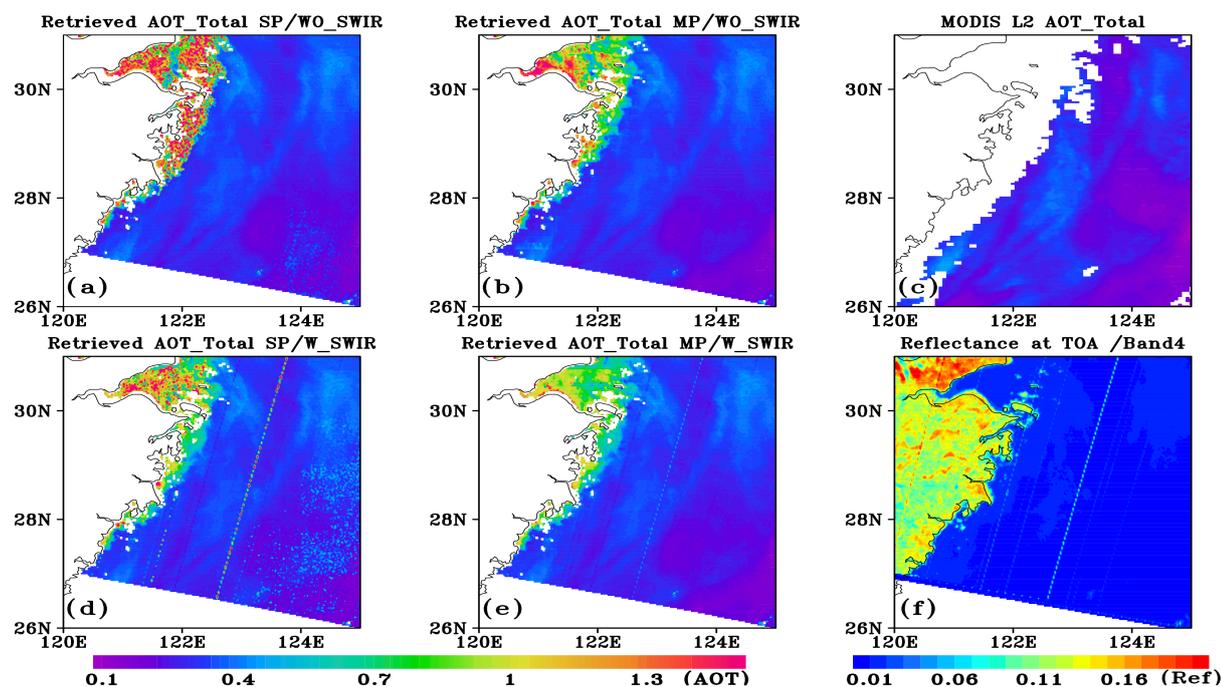
Figure 7: Comparison of CAI-retrieved total AOT by the single-pixel method without/with the SWIR band, i.e., 1600nm, (a and d, respectively), with those from the multi-pixel method without/with the SWIR band (b and e, respectively), as well as the spatial distributions of MODIS/Aqua Level 2 AOT products (c) and satellite-received reflectance at band4 of CAI (f) on the December 3rd, 2013.
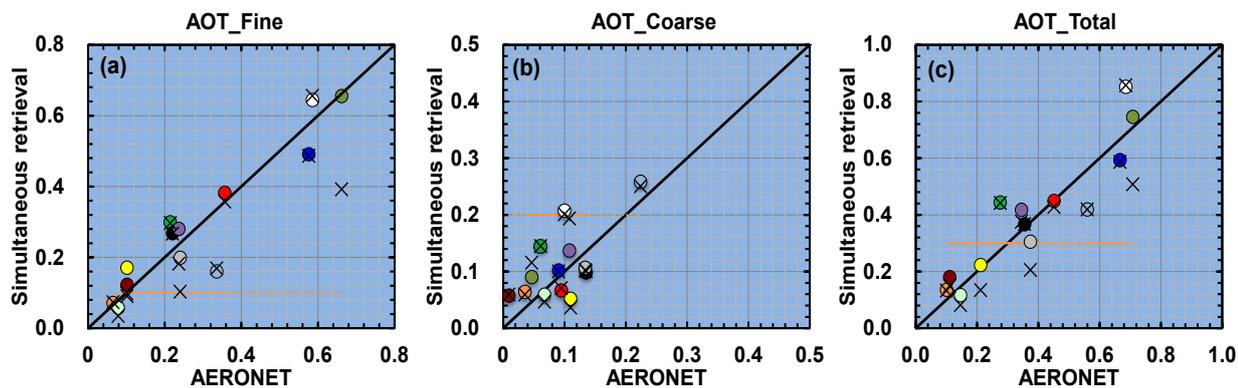
Figure 8: Comparison of retrieved AOT values for fine, coarse, and total aerosols at 500 nm from CAI with those from AERONET observations. Circles and crosses indicate the retrieved values at pixels closest to AERONET sites with/without multi-pixel method implementation, respectively. Orange dot lines denote apriori values.